

## NOTES AND CORRESPONDENCE

**Relationship between Low-Level Jet Properties and Turbulence Kinetic Energy in the Nocturnal Stable Boundary Layer**

ROBERT M. BANTA

*NOAA/Environmental Technology Laboratory, Boulder, Colorado*

YELENA L. PICHUGINA AND ROB K. NEWSOM

*Cooperative Institute for Research in the Atmosphere, Colorado State University, Fort Collins, Colorado*

13 October 2002 and 11 February 2003

## ABSTRACT

In the nighttime stable boundary layer (SBL), shear and turbulence are generated in the layer between the maximum of the low-level jet (LLJ) and the earth's surface. Here, it is investigated whether gross properties of the LLJ—its height and speed—could be used to diagnose turbulence intensities in this subjet layer. Data on the height and speed of the LLJ maximum were available at high vertical and temporal resolution using the high-resolution Doppler lidar (HRDL). These data were used to estimate a subjet layer shear, which was computed as the ratio of the speed to the height of the jet maximum, and a jet Richardson number  $Ri_j$ , averaged at 15-min intervals for 10 nights when HRDL LLJ data were available for this study. The shear and  $Ri_j$  values were compared with turbulence kinetic energy (TKE) values measured near the top of the 60-m tower at the Cooperative Atmosphere–Surface Exchange Study-1999 (CASES-99) main site. TKE values were small for  $Ri_j$  greater than 0.4, but as  $Ri_j$  decreased to less than  $\sim 0.4$ , TKE values increased, indicating that  $Ri_j$  does have merit in estimating turbulence magnitudes. Another interesting finding was that shear values tended to cluster around a constant value of  $0.1 \text{ s}^{-1}$  for TKE values that were not too small, that is, for TKE greater than  $\sim 0.1 \text{ m}^2 \text{ s}^{-2}$ .

**1. Introduction**

Turbulence and turbulent fluxes in the nocturnal stable boundary layer (SBL) are generated by vertical shear of the horizontal wind. Over relatively flat terrain, shear is generated by a low-level jet (LLJ) that forms after sunset as part of the evening boundary layer transition. As the LLJ accelerates after sunset, a layer of enhanced shear develops between the jet maximum and the earth's surface (Fig. 1a; see also, Fig. 18 in Poulos et al. 2002), generating turbulence in this layer (Smedman 1988; Nappo 1991; Mahrt 1998, 1999; Mahrt and Vickers 2002; Banta et al. 2002). The strength of the LLJ thus could act as a control on the magnitude of turbulence and turbulent fluxes in the SBL. This implies that it may be possible to diagnose turbulent fluxes in the SBL, provided the strength and height of the LLJ could be determined. Before undertaking the effort of studying how to determine LLJ properties from large-scale var-

iables for this purpose, however, it is first important to establish whether any relation actually exists between LLJ characteristics and turbulence below the jet.

To this end we used data from a high-resolution Doppler lidar to determine relevant LLJ properties and turbulence kinetic energy (TKE) measured near the top of a 60-m tower. The data were obtained during the Cooperative Atmosphere–Surface Exchange Study-1999 (CASES-99) intensive field campaign in October 1999. What is unique about the present study is that estimates of  $U_x$  and  $Z_x$  were available at high time and space resolution, where  $U_x$  is the speed of the LLJ maximum and  $Z_x$ , its height. Scan data were analyzed at 10-m height intervals, and many scans were repeated at  $\sim 30$  s intervals, so that LLJ characteristics were available at those resolutions. Here, we use the data that have been reanalyzed into mean values at 15-min intervals to provide estimates of subjet layer shear ( $U_x/Z_x$ ), as described by Banta et al. (2002). Shear estimates were then combined with stability estimates to calculate a jet Richardson number  $Ri_j$ . We compare these values with turbulence kinetic energy values at the upper levels of the 60-m tower erected for CASES-99.

---

*Corresponding author address:* Robert M. Banta, NOAA (ET2), 325 Broadway, Boulder, CO 80305.  
E-mail: robert.banta@noaa.gov

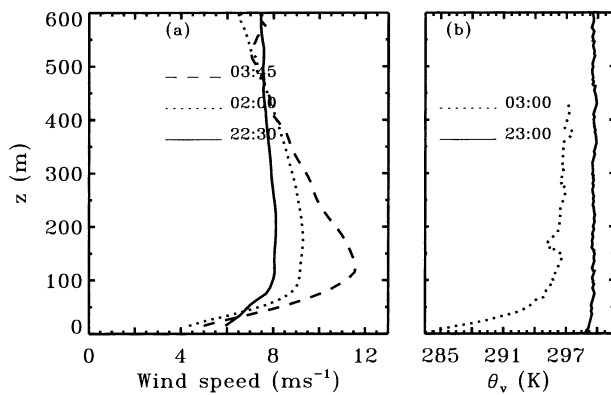


FIG. 1. (a) Vertical profiles of the along-wind component of the wind speed measured by HRDL on the night of 22–23 Oct (Julian night 296 UTC). Profiles show the development of an LLJ profile from a late-afternoon mixed-layer profile (solid line) to an LLJ profile during the nighttime hours (dotted line) by acceleration of the flow above 100 m AGL. (b) Potential temperature profiles from rawinsonde at Leon, Kansas 10 km from the main CASES-99 site, for the night of 22–23 Oct.

As in our previous LLJ study, we are interested in the first wind maximum above the surface. The vertical profile of the mean along-wind component  $U(z)$  was often nearly linear below this jet maximum (or “nose”) as shown in Fig. 2, so that the ratio  $U_x/Z_x$  (dashed lines in Fig. 2) is a reasonable estimate of the shear in this

layer. Also Fig. 1b and similar plots in Poulos et al. (2002, see their Figs. 11 and 18) show that the potential temperature profile  $\theta(z)$  was often roughly linear in the SBL between the surface layer and the nocturnal inversion top, although considerable fine structure was generally present. We assume for this study that  $\theta$  measured at 5 and 55 m on the tower gave reasonably representative estimates of the static stability ( $\partial\theta/\partial z$ ) below the top of the surface-based nocturnal inversion.

## 2. Instrumentation and analysis procedures

The CASES-99 experiment was described by Poulos et al. (2002). Instrumentation for this study includes the high-resolution Doppler lidar (HRDL) developed by the Environmental Technology Laboratory (ETL) of the National Oceanic and Atmospheric Administration (NOAA) and the aspirated temperature and sonic anemometers on the 60-m tower at the CASES-99 main site. HRDL was described by Grund et al. (2001) and Wulfmeyer et al. (2000), and its use in CASES-99 was discussed by Blumen et al. (2001), Banta et al. (2002), Newsom and Banta (2003), Poulos et al. (2002), and Sun et al. (2002, 2003). HRDL analysis procedures followed those described in Banta et al. (2002), including the enhanced velocity–azimuth display (VAD) procedure for calculating the wind profile over 15-min intervals and the method for determining the height and

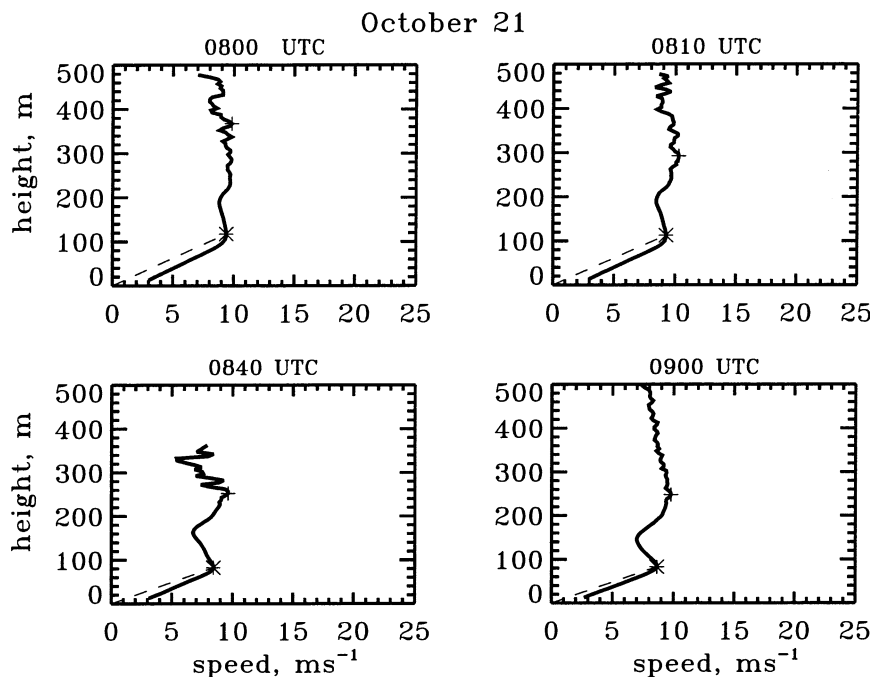


FIG. 2. Vertical profiles of the along-wind component of the wind calculated from vertical slice HRDL scan data. Profiles illustrate difficulties that can occur in attempting to determine  $Z_x$  and the importance of selecting the lowest wind-speed maximum in estimating subject shear. Plus symbols indicate maxima in profiles, and asterisks show height of lowest maximum, which would correspond to  $Z_x$ . Dashed line shows shear profile that would be calculated from bulk LLJ properties  $U_x/Z_x$ .

speed of the first wind speed maximum ( $Z_x$  and  $U_x$ , respectively).

The tower instrumentation used in this study included sonic anemometers (20 Hz) for the TKE calculation and the slow-response (recorded at 1 Hz) aspirated temperature sensors at 5 and 55 m AGL for the vertical  $\theta$  gradient. The slow-response instrument was chosen for the temperature measurement because of its accuracy and its temporal smoothing characteristics. Poulos et al. (2002) give an example of how the response characteristics of this sensor compared with the other two (thermocouple and sonic) sensors used during CASES-99 (see their Fig. 5). Occasionally the measurement at 55 m was unavailable, in which case the sensor at 50 m was used, and the vertical separation was adjusted accordingly in the lapse-rate calculation.

We calculated TKE using the 20-Hz sonic anemometer data at the 45-, 50-, and 55-m levels. The calculation of TKE under stable conditions presents problems because the turbulence is generally nonstationary. Vickers and Mahrt (2003) found that the most effective way to calculate heat and momentum fluxes was to use a two-step process consisting of 1) calculating the fluxes for time intervals corresponding to a gap in the cospectra, which for the CASES-99 dataset tended to occur at  $\sim 100$  s, and then 2) performing a simple average of the values from these shorter segments over a larger interval of  $\sim 1$  h. But, since the velocity power spectra that we looked at did not show a consistent spectral gap, we tried several approaches to calculating TKE. First we calculated the values over the 1-, 3-, 5-, 7-, 9-, and 11-min interval centered on the middle of each 15-min period for which  $U_x$  and  $Z_x$  had been calculated. Then we tried dividing the time series into 1-min segments and calculated the TKE for each segment, roughly following the Vickers–Mahrt procedure to account for nonstationarity. The TKE for these segments was then further averaged for the 3, 5, 7, 9, and 11 temporal segments centered on each 15-min interval of the LLJ data. In each of these cases, we then averaged the resulting TKE values in the vertical for the 45-, 50-, and 55-m tower levels. For the analysis performed here, each of these procedures yielded results that were similar. Thus, for this compositing study, the results proved rather insensitive to the precise method of averaging and TKE calculation for the procedures we tried. The results we present were from 1-min-averaged segments further averaged over five segments, that is, over a 5-min period in the middle of each 15-min block.

Because  $Z_x$  was often between 80 and 150 m, estimates of TKE at  $\sim 50$  m were often in the middle of the subject shear layer. For example, Newsom and Banta (2003) found an inflection point in the velocity profile at about this level in their 6 October 1999 case. It thus seemed to be a good level to sample for turbulence for the CASES-99 dataset—when turbulence was present in the subject layer it often occurred at this level.

A measure of dynamic stability is the gradient Richardson number

$$Ri = \frac{g}{\theta} \frac{\Delta\theta/\Delta z}{(\Delta U/\Delta z)^2}. \quad (1)$$

The flow can become turbulent when the value of  $Ri$  is less than critical, which depends on the flow characteristics. For purposes of this study,  $Ri$  has been modified into a bulk jet Richardson number, where the shear in the denominator is estimated from the speed and height of the jet:

$$Ri_j = \frac{g}{\theta} \frac{\Delta\theta/\Delta z}{(U_x/Z_x)^2}. \quad (2)$$

The major measurement uncertainty in the calculation of  $Ri_j$  was the height of the jet  $Z_x$  in the subject-shear calculation. The jet speed generally varied slowly in time and often tended to be relatively constant with height, producing periods when  $Z_x$  was ambiguous or otherwise difficult to determine, as shown in Fig. 2. Other sources for uncertainty include the following: 1) directional shear was not available from the vertical-slice HRDL scan data (and thus was not included in the bulk shear and  $Ri_j$  estimates), 2) turbulence may have been present but at levels other than the 45–55-m levels being sampled, and 3) the 5–55-m level might not give representative estimates of the subject  $\partial\theta/\partial z$ . We also note that (apart from the missing directional shear) the shear determined in this manner is a slight overestimate of the actual shear in the measured profile, as is evident from the dashed lines in Fig. 2. The overestimate was due in part to a departure from linearity within a few meters of the surface, where  $\partial U/\partial z$  (and also  $\partial\theta/\partial z$ ) becomes very large.

The 13 nights for which HRDL LLJ data were available are tabulated in our CASES-99 LLJ study (Banta et al. 2002). Two nights were excluded because of insufficient TKE data availability. The only other night excluded here was that of 17–18 October (Julian night 291, UTC), when the significant turbulence episodes were caused by density currents and solitary waves (Sun et al. 2002, 2003) rather than LLJ-generated shear, and thus do not apply to our analysis. We generated time series for each night; two examples are shown in Figs. 3–4 that illustrate the behavior of the shear, stability, and  $Ri_j$  for each night. Also shown plotted with  $Ri_j$  is the tower-measured TKE.

### 3. Results

The time series in Figs. 3–4 show two different patterns, one (25 October; Fig. 3) that has a strong LLJ and TKE levels exceeding  $0.4 \text{ m}^2 \text{ s}^{-2}$  for most of the night, and one (26 October; Fig. 4) with a weak LLJ and small TKE ( $< 0.05 \text{ m}^2 \text{ s}^{-2}$ ) for most of the night. Scatter diagrams of TKE versus  $Ri_j$  were generated for each night when LLJ data were available from HRDL.

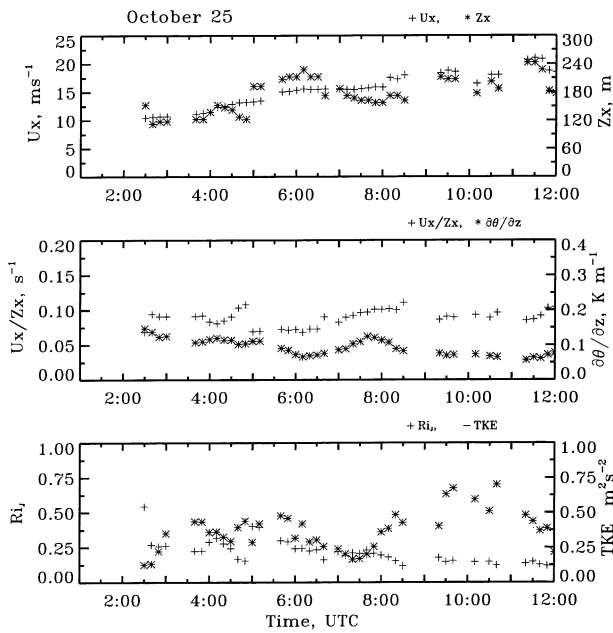


FIG. 3. Time series of LLJ characteristics  $U_x(+)$  and  $Z_x(*)$  (top), mean shear (+) and  $\theta$  gradient (\*) (middle), and calculated  $Ri_j(+)$  (bottom) from 15-min-averaged LLJ data from HRDL for 25 Oct (Julian night 298 UTC). Bottom also shows TKE values (\*) measured by sonic anemometers near the top of the 60-m CASES-99 main tower, as described in the text.

The scatter diagram for the two sample nights is shown in Fig. 5. On 25 October, the high TKE values appeared mostly between  $Ri_j$  values of 0.1 and 0.3. On 26 October, the large  $Ri_j$  values observed (mostly  $>3$ ) were associated with low TKE values.

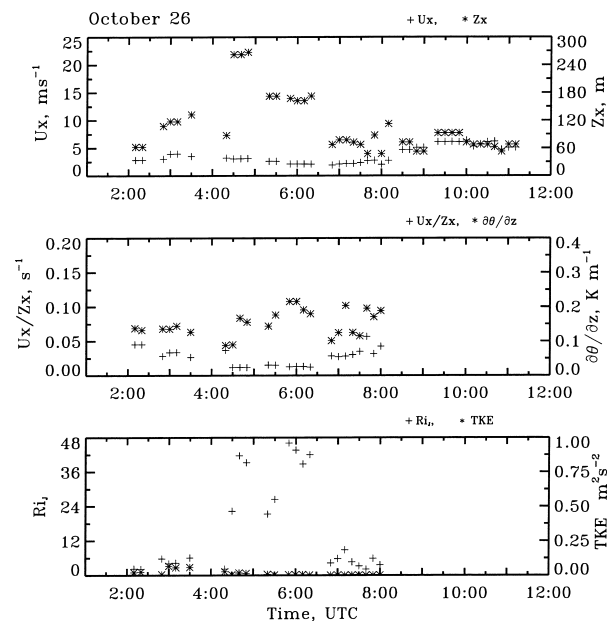


FIG. 4. Same as in Fig. 3, except for 26 Oct (Julian night 299 UTC).

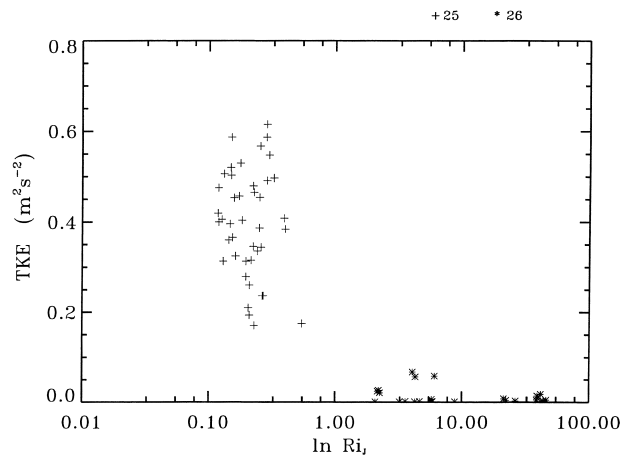


FIG. 5. Scatter diagram of  $Ri_j$  vs TKE for 25 Oct (+) and 26 Oct (\*), plotted on a logarithmic scale for  $Ri_j$ .

In comparing the LLJ data and the TKE data, we first sought to determine whether the shear itself could be used as a predictor of turbulence activity. Figure 6 shows the tower TKE plotted against the subjct shear  $U_x/Z_x$ . Interestingly, for values of TKE greater than  $\sim 0.1 \text{ m}^2 \text{ s}^{-2}$ , the values cluster around a shear value of  $0.1 \text{ s}^{-1}$ . This suggests that for a given jet speed, the LLJ nose adjusted via turbulent mixing to a height such that the shear was maintained at this value. We note that this relationship broke down when TKE levels were small, presumably because the amount of mixing required to maintain constant shear at the appropriate value did not occur. We also note that preliminary analysis of summertime LLJ data from Doppler lidar near Nashville, Tennessee, indicate higher jet maxima for a given wind speed. Here the region is forested and has higher moisture and aerosol loading, suggesting that the maintained shear value may be related to surface effects such as roughness or radiative cooling. It is tempting to con-

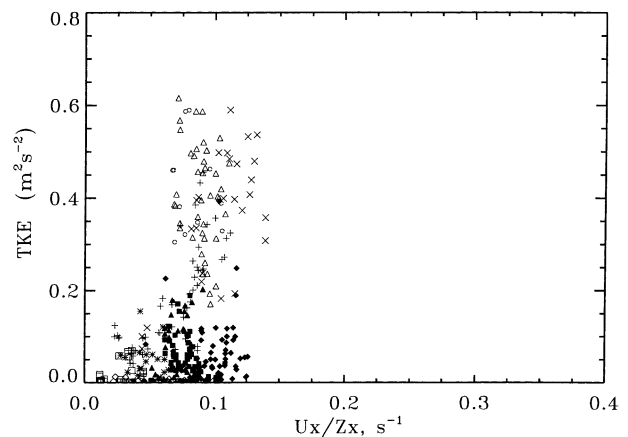


FIG. 6. Scatter diagram of HRDL-measured subjct shear  $U_x/Z_x$  vs tower-measured TKE for entire sample of 10 nights. Different symbols represent different nights of CASES-99; exact dates are not important for this study.

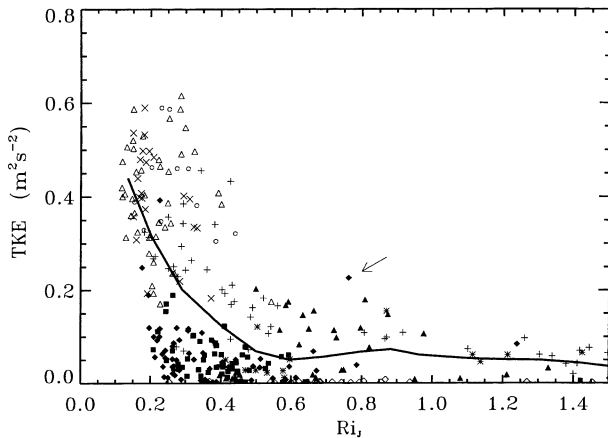


FIG. 7. Scatter diagram of  $Ri_j$  vs TKE (as in Fig. 5) for entire sample of 10 nights. As in Fig. 6, shear estimates in  $Ri_j$  calculation were from HRDL measurements of LLJ properties. Different symbols represent different nights of CASES-99, as in Fig. 6. Data were divided into  $Ri_j$  intervals of 0.05, and the mean TKE was calculated for each interval. The solid line connects these mean TKE values.

clude from this lack of sensitivity of TKE to shear that shear by itself has no predictive value in determining turbulence magnitude, but it is important to note that this is true only in the bulk sense being considered here. Newsom and Banta (2003), for example, showed that over a shorter timescale and smaller vertical interval, it was a local increase in shear that triggered a turbulence event caused by shear-instability waves.

The scatter diagram of TKE versus  $Ri_j$  for the entire sample of 10 nights is given in Fig. 7. For stable  $Ri_j$  values greater than 0.4, TKE values were low, as in Fig. 5 for the light-wind night. As  $Ri_j$  values decreased below 0.4, turbulence levels increased, as expected. We note that, owing to the scatter introduced by the uncertainties in estimating  $Z_x$  and other sampling issues (as described previously), the data presented are not inconsistent with a value of  $Ri_j$  of 0.25, below which the TKE began to increase to values greater than  $0.1 \text{ m}^2 \text{ s}^{-2}$ . In this case, for values below the  $\sim 0.4$  or so threshold, TKE did indicate sensitivity to  $Ri_j$ . The solid line in Fig. 7, which connects the mean TKE values for each 0.05 interval of  $Ri_j$ , clearly shows TKE tending to increase as  $Ri_j$  decreases.

It is ordinarily inappropriate to find individual data points significant in analyses such as Fig. 7, but one data point in this figure is of particular interest. The anomalous point indicating relatively high TKE values ( $>0.2 \text{ m}^2 \text{ s}^{-2}$ ) at  $Ri_j \sim 0.7$  (indicated by the arrow) represents conditions during the shear-instability event on 6 October [intensive observation period (IOP)2] described by Newsom and Banta (2003) and Blumen et al. (2001). As pointed out in the Newsom–Banta analysis, the overturning wave activity produces a decrease in the shear of the averaged wind profile during the course of the event, and thus an increase in  $Ri$  compared with before and after the event. The effect appeared here

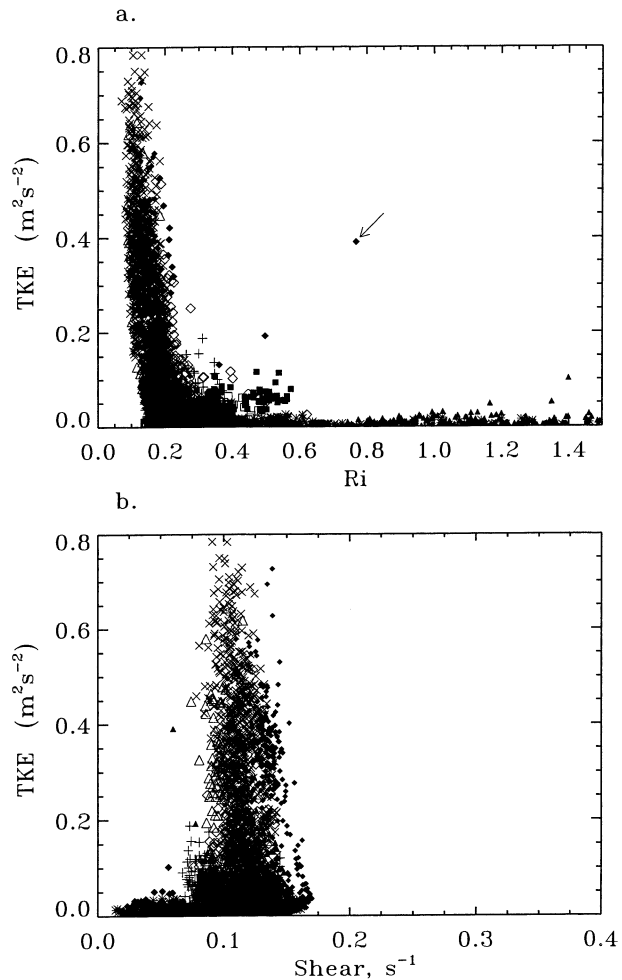


FIG. 8. Scatter diagram of (a) gradient  $Ri$  vs TKE and (b) tower-measured shear vs TKE for the same sample of 10 nights as in Figs. 6–7. The shear in the  $Ri$  calculation and in (b) was a bulk value measured between 5 and 55 m on the tower.

as high TKE at an unusually high  $Ri$ . This illustrates a basic problem with the high  $Ri$  very stable boundary layer as defined by Mahrt (1999); that is, the mixing that does occur is in intermittent patches or events of relatively small scale. During the mixing events, averaged profiles may have already been modified by the event and thus may be less useful for diagnosing the existence of the turbulent mixing activity in these cases.

Much of the scatter in both Figs. 6 and 7 arises from the difficulty of estimating LLJ parameters when the height of the maximum  $Z_x$  is ambiguous or ill defined (see section 2), which leads to uncertainties in the estimate of  $U_x/Z_x$ . In these cases,  $Z_x$  was generally estimated to be too high, leading to low shear estimates and to  $Ri$  values that were too big. It is of interest to determine what might result if we could obtain a better estimate of the subjet shear, using tower data, for example. Figure 8 shows the same data as presented in Figs. 6 and 7, except  $\Delta U$  in the numerator of the shear

calculation was computed from the sonic anemometers at the 5- and 55-m levels on the CASES-99 main tower, and  $\Delta z$  in the denominator from the vertical separation of the sensors (50 m). The overall results are the same as for the LLJ-determined estimates, except the fit is much tighter, with less scatter. The shear value about which the data tend to cluster in the shear plot (Fig. 8b) appears to be somewhat greater than  $0.1 \text{ s}^{-1}$ , although  $U_x/Z_x$  was a slight overestimate of the shear. In the  $Ri$  plot (Fig. 8a), the  $Ri$  value below which TKE begins to significantly increase is more clearly closer to 0.25 than in Fig. 7. The *only* difference between Fig. 7 and Fig. 8a is that the shear value used for Fig. 8a is a much better estimate for the shear in the linear portion of the subject  $U$  profile illustrated in Fig. 2. We note that this plot is quite consistent with expectation. For example, Mahrt (1987) found similar behavior for the vertical velocity variance calculated from aircraft data, although at a higher critical  $Ri$ .

#### 4. Discussion and conclusions

A significant control on the turbulence and turbulent fluxes in the nighttime SBL over nonmountainous terrain is the shear generated beneath the LLJ. Although we have paid considerable attention to LLJ properties in this paper, the contribution of the jet is to produce a region of enhanced shear that is confined in the vertical, which can lead to turbulence production in the subject layer. Bulk properties of the LLJ—its speed and height—may be available from numerical weather prediction (NWP) model output or via analysis of larger-scale quantities, such as horizontal pressure gradients, thermal winds, and ageostrophic wind components. In this study we have shown that these bulk LLJ properties are useful for estimating the subject shear, which can then be used to calculate  $Ri_j$ , which in turn has been shown to be related to turbulence measures in the subject layer.

An important implication is that if the strength and height of the LLJ can be accurately determined or predicted, they could be used to diagnose turbulence effects in the subject layer of the SBL. Conversely, if the strength and height are *not* accurately determined, the vertical turbulent mixing properties will not be accurately represented either. Current NWP models do not routinely produce reliable LLJ characteristics, presumably because of poor representation of vertical mixing under stable conditions, as pointed out by Mahrt (1998), Banta et al. (2002), and others. For proper representation of  $Ri_j$ , it is also necessary to get the stability  $\partial\theta/\partial z$  right near the surface. This involves proper representation of longwave radiation and the budgets of net radiation and energy at the surface, and these too are concerns in current-generation NWP models (Zamora et al. 2003; Zhong and Fast 2003).

For this dataset the subject shear value tended to cluster around a constant value when some turbulence was pres-

ent (e.g., TKE exceeded  $\sim 0.1 \text{ m}^2 \text{ s}^{-2}$ ). This surprising result may offer another approach and give further hope for calculating turbulence, if verified by other datasets. It would mean that  $Ri_j$  could be calculated with some accuracy if the stability alone could be well represented, that is, if the radiation and energy budgets were accurately calculated at and near the surface.

Besides this constant-shear approach, the present study indicates that it would be worthwhile to investigate how to determine gross LLJ properties from larger-scale meteorological quantities, such as the ageostrophic wind profile, surface cooling rates, and the vertical profile of the horizontal pressure gradient (including its temporal variation), for the purpose of relating these properties to subject turbulence and fluxes. At the other end of the spectrum, it is also important to investigate how subject turbulence relates to turbulent exchange processes at the surface. The surface acts as a source or sink in the budgets of many key quantities, including momentum, heat, and trace species, and so an important ultimate goal should be to accurately represent these surface fluxes. The bulk procedure described here discriminates between the moderately stable boundary layer at  $Ri_j < 0.25$ – $0.30$  or so, where turbulent mixing is continuous, and the very stable boundary layer at higher values of  $Ri_j$ , where the turbulence is intermittent, as defined by Mahrt (1999). This suggests that turbulence properties can be diagnosed from gross LLJ properties for the moderately stable case. Under very stable conditions, however, where mixing is patchy, the mean mixing over a region depends on other factors, which may include the size (areal coverage), spatial frequency, and strength or mixing effectiveness of the turbulent patches. As shown by the anomalous point in Figs. 7–8, representing these fluxes as functions of larger-scale quantities is difficult, and addressing this problem is an important priority.

*Acknowledgments.* Funding for analysis and field measurements was provided by the Army Research Office under proposal 40065-EV and the Center for Geosciences/Atmospheric Research at Colorado State University. The National Science Foundation Grant ATM-9908453 (HRDL) and the DOE National Renewable Energy Laboratory IA DE-AI36-01GO11066 also provided funding for the field measurements and/or analysis. We appreciate helpful discussions with L. Mahrt and D. Vickers on the TKE calculation procedure. The authors are indebted to J. Otten, Dr. W. Eberhard, and M. Pichugin for contributions to HRDL data acquisition; Dr. V. Wulfmeyer, S. Sandberg, J. George, Dr. W. A. Brewer, A. Weickmann, R. Richter, and Dr. R. M. Haresty for HRDL preparation and setup; Dr. J. Sun, S. Burns, Dr. S. Oncley, and N. Chamberlain for tower and sounding data; Dr. W. A. Brewer and B. McCarty for contributions to the analysis of the scan data; Lisa S. Darby and Robert J. Zamora for reviews of the manuscript; Dr. G. Poulos, Dr. W. Blumen, and Dr. D. Fritts

for organizing the CASES-99 field project; and J. Klazura for local arrangements.

## REFERENCES

- Banta, R. M., R. K. Newsom, J. K. Lundquist, Y. L. Pichugina, R. L. Coulter, and L. J. Mahrt, 2002: Nocturnal low-level jet characteristics over Kansas during CASES-99. *Bound.-Layer Meteor.*, **105**, 221–252.
- Blumen, W., R. M. Banta, S. P. Burns, D. C. Fritts, R. K. Newsom, G. S. Poulos, and J. Sun, 2001: Turbulence statistics of a Kelvin-Helmholtz billow event observed in the nighttime boundary layer during the CASES-99 field program. *Dyn. Atmos. Oceans*, **34**, 189–204.
- Grund, C. J., R. M. Banta, J. L. George, J. N. Howell, M. J. Post, R. A. Richter, and A. M. Weickmann, 2001: High-resolution Doppler lidar for boundary-layer and cloud research. *J. Atmos. Oceanic Technol.*, **18**, 376–393.
- Mahrt, L., 1987: Grid-averaged surface fluxes. *Mon. Wea. Rev.*, **115**, 1550–1560.
- , 1998: Stratified atmospheric boundary layers and breakdown of models. *J. Theor. Comput. Fluid Dyn.*, **11**, 263–280.
- , 1999: Stratified atmospheric boundary layers. *Bound.-Layer Meteor.*, **90**, 375–396.
- , and D. Vickers, 2002: Contrasting vertical structures of nocturnal boundary layers. *Bound.-Layer Meteor.*, **105**, 351–363.
- Nappo, C. J., 1991: Sporadic breakdowns of stability in the PBL over simple and complex terrain. *Bound.-Layer Meteor.*, **54**, 69–87.
- Newsom, R. K., and R. M. Banta, 2003: Shear-flow instability in the stable nocturnal boundary layer as observed by Doppler lidar during CASES-99. *J. Atmos. Sci.*, **60**, 16–33.
- Poulos, G., Coauthors, 2002: CASES-99: A comprehensive investigation of the stable nocturnal boundary layer. *Bull. Amer. Meteor. Soc.*, **83**, 555–581.
- Smedman, A. S., 1988: Observations of a multi-level turbulence structure in a very stable atmospheric boundary layer. *Bound.-Layer Meteor.*, **44**, 231–253.
- Sun, J., and Coauthors, 2002: Intermittent turbulence in stable boundary layers and its relationship with density current. *Bound.-Layer Meteor.*, **105**, 199–219.
- , and Coauthors, 2003: Intermittent turbulence in stable boundary layers and the processes that generate it. *Bound.-Layer Meteor.*, **106**, in press.
- Vickers, D., and L. Mahrt, 2003: The cospectral gap and turbulent flux calculations. *J. Atmos. Oceanic Technol.*, **20**, 660–672.
- Wulfmeyer, V. O., M. Randall, W. A. Brewer, and R. M. Hardesty, 2000: 2  $\mu\text{m}$  Doppler lidar transmitter with high frequency stability and low chirp. *Opt. Lett.*, **25**, 1228–1230.
- Zamora, R. J., and Coauthors, 2003: Comparing MM5 radiative fluxes with observations gathered during the 1995 and 1999 Nashville southern oxidants studies. *J. Geophys. Res.*, **108**, 4050, doi: 10.1029/2002JD002122.
- Zhong, S., and J. Fast, 2003: An evaluation of the MM5, RAMS, and Meso-Eta models at subkilometer resolution using VTMX field campaign data in the Salt Lake Valley. *Mon. Wea. Rev.*, **131**, 1301–1322.